



Synergistically enhanced photocatalytic activity of graphitic carbon nitride and WO_3 nanohybrids mediated by photo-Fenton reaction and H_2O_2



Minji Yoon ^{a,1}, Youngtak Oh ^{b,c,1}, Sugyeong Hong ^d, June Sang Lee ^a, Ramireddy Boppella ^a, Sun Hee Kim ^d, Filipe Marques Mota ^{a,*}, Sang Ouk Kim ^{b,**}, Dong Ha Kim ^{a,d,e,*}

^a Department of Chemistry and Nano Science, Ewha Womans University, 52, Ewhayeodae-gil, Seodaemun-gu, Seoul 03760, Republic of Korea

^b Department of Materials Science and Engineering, Korea Advanced Institute of Science and Technology, 335 Gwahangno, Yuseong-gu, Daejeon 34141, Republic of Korea

^c Center for Environment, Health, and Welfare Research, Korea Institute of Science and Technology, Seoul 02792, Republic of Korea

^d Western Seoul Center, Korea Basic Science Institute, University-Industry Cooperation Building, 150 Bukahyun-ro, Seodaemun-gu, Seoul 03759, Republic of Korea

^e Division of Chemical Engineering and Materials Science, College of Engineering, Ewha Womans University, 52, Ewhayeodae-gil, Seodaemun-gu, Seoul 03760, Republic of Korea

ARTICLE INFO

Article history:

Received 4 October 2016

Received in revised form 9 January 2017

Accepted 15 January 2017

Available online 16 January 2017

Keywords:

Visible light photocatalysis

Photo-Fenton reaction

Electron paramagnetic resonance

Carbon nitride

Tungsten oxide

ABSTRACT

The development of solar energy conversion in the production of fuels, water splitting and water purification systems, has become an important sidestep for traditional fossil energy. Herein we have investigated the coupling effect of a Photo-Fenton system on a conventional photocatalytic reaction with a novel Fe-doped $\text{C}_3\text{N}_4/\text{WO}_3$ hybrid structure. The decomposition of *p*-nitrophenol was selected as a model reaction in the context of the degradation of organic pollutants. Heterojunction nanocomposites consisting of $\text{g-C}_3\text{N}_4$ nanosheets and WO_3 nanoparticles were shown to facilitate the separation of photo-induced electron and hole pairs. The photocatalytic activity was further maximized as a result of a synergism of the 'Photo-Fenton cycle' with Fe(II) or Fe(III)-doping in the presence of H_2O_2 to generate additional hydroxyl radicals. As a result, after 4 h under visible light the degradation of *p*-nitrophenol could be remarkably enhanced from 10 to 90% compared to the $\text{g-C}_3\text{N}_4$ reference. To the best of our knowledge, this is the first time such a striking increase is reported with a Photo-Fenton system applied in the present photocatalytic system. The significance of the presence of hydroxyl radicals in the photo-Fenton performance of Fe-doped $\text{C}_3\text{N}_4/\text{WO}_3$ was assessed by scavenger and fluorescence tests. Additional light was shed into the reaction mechanism via spin trapping enabled by *in-situ* electron paramagnetic resonance.

© 2017 Elsevier B.V. All rights reserved.

1. Introduction

Foreseen reduced fossil fuels supplies and current environmental concerns have italicized the importance of developing high efficiency green energy sources and eco-friendly methods for

replacing traditional fossil energy [1–3]. Solar energy has been shown to drive a number of chemical processes of prime importance through a photocatalytic mechanism, including production of fuels, water splitting and water purification [4–7]. Continuous exploratory strategies have been employed to improve the photocatalytic activity of semiconductor photocatalysts *via* suitable facets [8,9], doping [3,6,10–12], noble metal loading [13–17] and hybrid composites [14,18–22]. In particular, carbon nitride ($\text{g-C}_3\text{N}_4$) with large surface area and high chemical stability has emerged as a promising metal-free photocatalyst [23–31]. Its low band gap (2.7 eV) facilitates light absorption up to 460 nm, highlighting $\text{g-C}_3\text{N}_4$ as a valuable candidate for solar energy conversion [32], organic pollutant degradation [33], hydrogen production [34] and carbon dioxide storage [35]. The efficiency of $\text{g-C}_3\text{N}_4$ has however remained limited for practical applications in view of the high

* Corresponding authors at: Department of Chemistry and Nano Science, Ewha Womans University, 52, Ewhayeodae-gil, Seodaemun-gu, Seoul, 03760, Republic of Korea.

** Corresponding author at: Department of Materials Science and Engineering, Korea Advanced Institute of Science and Technology, 335 Gwahangno, Yuseong-gu, Daejeon 34141, Republic of Korea.

E-mail addresses: filiptmarques.m@gmail.com (F. Marques Mota), sangouk.kim@kaist.ac.kr (S.O. Kim), dhkim@ewha.ac.kr (D.H. Kim).

¹ The authors contributed equally to this work.

recombination rate of photo-excited electron-hole pairs [36]. A number of sidestep approaches, e.g., metal doping [37–39], non-metal doping [40,41], morphology control [42] and coupling with other materials [43,44], has hence been contemplated. Particularly, doping of iron (Fe) onto the surface of g-C₃N₄ was proposed to intensively enhance its photocatalytic performance due to the improved optical absorption and low recombination rate.

In the context of the degradation of organic pollutants, Fenton and Photo-Fenton systems in the presence of Fe species and hydrogen peroxide have been broadly investigated as effective advanced oxidation processes (AOPs). H₂O₂ has been reported to rapidly react with dissolved Fe species producing reactive hydroxyl radicals, which oxidize the organic compounds [45–48]. Notwithstanding the numerous reports with a focus on this topic [49,50], one of the challenges to monitor Photo-Fenton processes lies in the complexity of an effective quantitative analysis of the highly reactive hydroxyl radicals involved in the reaction. In particular we believe that a detailed description of the Photo-Fenton mechanism is of prime importance in the case of novel hybrid materials with improved catalytic performance [51]. In this context a number of reports have emerged in recent years focusing on scavenger tests [52], photoluminescence data [53] and spin trapping enabled by electron paramagnetic resonance (EPR) analysis [54].

Herein, recent relevant reports inspired the development of unconventional g-C₃N₄/WO₃ hybrid nanocomposites doped with Fe(II) or Fe(III) to remarkably enhance the photocatalytic activity, based on the synergistic combination of photo-oxidation and Fenton reaction. We recently investigated the precise description of local coordination of metal at carbon nitride interface as well as the corresponding electronic structural identity, via both solid state nuclear magnetic resonance spectroscopy and density functional theory calculation [55,56]. The formed heterojunction has been suggested to improve the separation of electron and hole pairs, which leads to the enhanced photocatalytic efficiency [57]. Here we investigated the photocatalytic performance of Fe-doped g-C₃N₄ and WO₃ nanoparticles [35] hybrid materials in the degradation of p-nitrophenol (PNP), as a representative hazardous waste in industrial wastewaters, with high stability and solubility in water. The results were corroborated using scavenger and fluorescence tests, with EPR measurements shedding additional light in the postulated reaction mechanism involving OH radicals generated by simultaneous photo-oxidation and photo-Fenton processes.

2. Experimental

2.1. Synthesis of the samples

Ammonium tungstate, dicyandiamide, iron halid, terephthalic acid, *tert*-butyl alcohol, para-nitro phenol, 5,5-Dimethyl-1-pyrroline N-oxide were purchased from Sigma-Aldrich. For the synthesis of the Fe-doped C₃N₄ samples, 12.6 mg of Fe(II)Cl₂ or alternatively Fe(III)Cl₃ were physically mixed with 1 g of dicyandiamide and ground under inert atmosphere. The samples were then heated under N₂ flow at 600 °C for 4 h, following a heating rate of 2.5 °C min⁻¹. Detailed characterization of the Fe-doped g-C₃N₄ has been reported elsewhere [55]. WO₃ nanoparticles were synthesized by solid-state decomposition of ammonium tungstate at 550 °C for 4 h [58]. The resulting powder was consecutively washed with water and ethanol. The process was repeated twice, after which the resulting solid was dried at 60 °C for 6 h. For the preparation of the hybrid materials, 0.01 g of WO₃ and 0.1 g of g-C₃N₄ (or Fe-doped C₃N₄) were effectively ground together for 30 min [59]. The resulting powder was then heated at 450 °C in a furnace for 4 h, following a heating rate of 20 °C min⁻¹.

2.2. Characterization techniques

The synthesized hybrids were investigated using scanning electron microscopy (SEM, JEOL JSM6700-F) and transmission electron microscopy (TEM, JEOL JSM2100-F) at 100 kV. X-ray diffraction (XRD) patterns were recorded using Cu-K α radiation (D/max RA, Rigaku Co.). UV-vis absorbance and diffuse reflectance spectra (DRS) were measured using a Sinco S-4100 spectrometer. A Perkin Elmer LS 55 fluorescence spectrometer was used to obtain photoluminescence spectra of the 2-hydroxyterephthalic acid at an excitation wavelength of 365 nm. X-band continuous-wave EPR spectra were obtained using a Bruker EMX/Plus spectrometer equipped with a dual-mode cavity (ER 4116DM). Atomic force microscopy (AFM) images were obtained using a Dimension 3100 scanning force microscope in tapping mode (Digital Instrument). Electrochemical impedance spectroscopy (EIS) was performed using an IviumStat electrochemical workstation, at open circuit potential in a 10⁻²–10⁵ Hz frequency range, using a conventional three-electrode system. Indium-tin oxide (ITO) glass was selected as the working electrode, platinum wire as the counter electrode, and Ag/AgCl as the reference electrode. Both C₃N₄/WO₃ and C₃N₄ were grinded in isopropyl alcohol, and the homogeneous suspensions were deposited (20 μ l) on corresponding 0.5 cm² surface area of ITO.

2.3. Photo-Fenton degradation of PNP

The photo-Fenton degradation of *p*-nitrophenol (PNP) was evaluated under UV and visible light illumination. Each sample (5 mg) was suspended in a PNP solution (30 ml, 10 ppm) and magnetically stirred under dark conditions for 1 h. Samples were illuminated using a Xe lamp (200–2500 nm-range, Newport Co. Ltd., Model 66984) alternatively equipped with a 420 nm cut-off filter at 300 W as a visible light source. H₂O₂ solution with optimized concentration (0.005 M) was fed to the system. Periodically collected samples were centrifuged (5000 rpm) during 10 min, and the supernatant solution analyzed by UV-vis spectroscopy. The photocatalytic activity of each sample was determined according to the gradual decrease of the characteristic peak of PNP at 400 nm, measured using a Varian Cary5000 UV-vis-NIR spectrophotometer.

The degradation of PNP under UV-vis light illumination in the absence of catalyst was confirmed negligible (Fig. S1), corroborating previous literature reports [60,61]. Similarly, the conversion of these Fe-doped hybrid materials remained minor in the absence of light even after 5 h (Fig. S2).

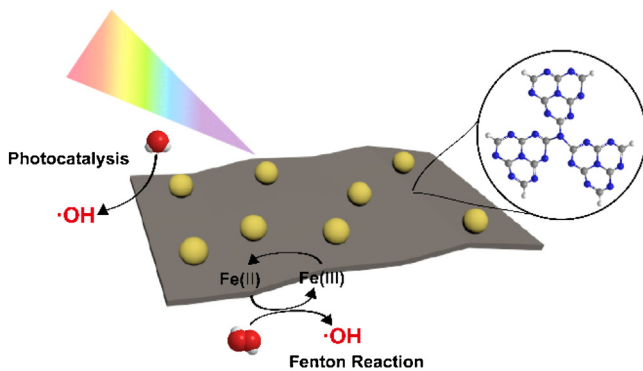
2.4. Analysis of hydroxyl radicals

2.4.1. Electron paramagnetic resonance (EPR) analysis

The evaluation of the effect of the presence of OH on the degradation of PNP was considered to shed light in the Photo-Fenton reaction mechanism. EPR tests were carried out in a similar way as described for the Photo-Fenton system. 5,5-dimethyl-1-pyrroline-N-oxide (DMPO) was selected as the spin-trapping reagent. Resulting hydroxyl radical-DMPO products (DMPO-•OH) were analyzed using a Bruker EMX/Plus spectrometer equipped with a dual-mode cavity under visible light illumination, as described before.

2.4.2. Scavenger test

To investigate the active hydroxyl radical species during the Fenton process, *tert*-butyl alcohol (TBA) was added to the catalytic system leading to the formation of *tert*-butanol (TBA-OH), following previous literature reports [62,63]. The scavenger test was then carried out as previously described for the photocatalytic degradation of PNP.



Scheme 1. Schematic illustration of the unconventional hybrid sample and a photo-Fenton reaction. (WO_3 nanoparticles (yellow) are represented deposited on thin C_3N_4 nanosheets (grey). (For interpretation of the references to colour in this figure legend, the reader is referred to the web version of this article.)

2.4.3. Fluorescence test

The concentration of hydroxyl radical species generated during the Photo-Fenton reaction was estimated in the presence of a terephthalic acid (TA) probe, through the formation of the highly fluorescent 2-hydroxyterephthalic acid (TA- $\cdot\text{OH}$) detected at 435 nm [64]. The as-prepared catalyst powder was dispersed in 100 ml of TA/NaOH solution ($5 \times 10^{-4} \text{ mol L}^{-1}$, $2 \times 10^{-3} \text{ mol L}^{-1}$ respectively) under visible light illumination.

3. Results and discussion

The unconventional heterojunction nanohybrid consisting of Fe-doped $\text{g-C}_3\text{N}_4/\text{WO}_3$ along with photo-oxidation and Photo-Fenton reaction is depicted in Scheme 1. $\text{g-C}_3\text{N}_4$ nanosheets were prepared using dicyandiamide, with Fe species being then doped via iron halide treatment. In the preparation of our Fe-doped $\text{g-C}_3\text{N}_4/\text{WO}_3$ nanostructure, $\text{g-C}_3\text{N}_4$ (or Fe-doped C_3N_4) and WO_3 nanoparticles were firstly ground and heated at 450°C . The final nanostructure was exfoliated by sonication for 2 h and sequentially washed with water and ethanol.

3.1. Fe-doped $\text{g-C}_3\text{N}_4$

Fe-doped $\text{g-C}_3\text{N}_4$ materials were prepared as detailed in the Experimental Section. For a representative comparison of the photocatalytic data similar amounts of Fe(II) and Fe(III)-species were doped. The $\text{g-C}_3\text{N}_4$ reference and both corresponding Fe-doped samples were investigated by XRD (Fig. 1a). The strongest diffraction peaks of the $\text{g-C}_3\text{N}_4$ reference at 27.4° and 13.1° correspond to the (002) and (100) planes, and thus to the characteristic peaks of the aromatic systems and the interlayer structure packing, respectively [65]. AFM analysis of exfoliated C_3N_4 confirmed the presence of ultrathin sheets with thickness up to 5 nm (Fig. S3). Individual EDS elemental maps revealed a uniform distribution of N, C and Fe (Figs. 2, S4). XPS measurements confirmed the presence of both divalent and trivalent species in the samples evaluated in this study (Fig. S5). The amount of both di and trivalent Fe species estimated by Elemental Analysis was accounted to 0.90 and 0.94 wt.%, respectively. Collected UV-vis absorption spectra for the as-synthesized $\text{g-C}_3\text{N}_4$ nanosheets and corresponding Fe-doped counterparts are indicated in Fig. 1b. Both Fe(II)- and, in particular, Fe(III)-doped $\text{g-C}_3\text{N}_4$ unveiled a predominant absorbance increase under UV light illumination. The band gap energy of each sample was determined according to the corresponding Kubelka-Munk plots (Fig. 1c) and Eq. (1), with α , the absorption coefficient, h , Planck constant, ν , the frequency, E_g , the band gap energy, A , a constant, and n , as an additional constant accounting for the type of optical transitions [66].

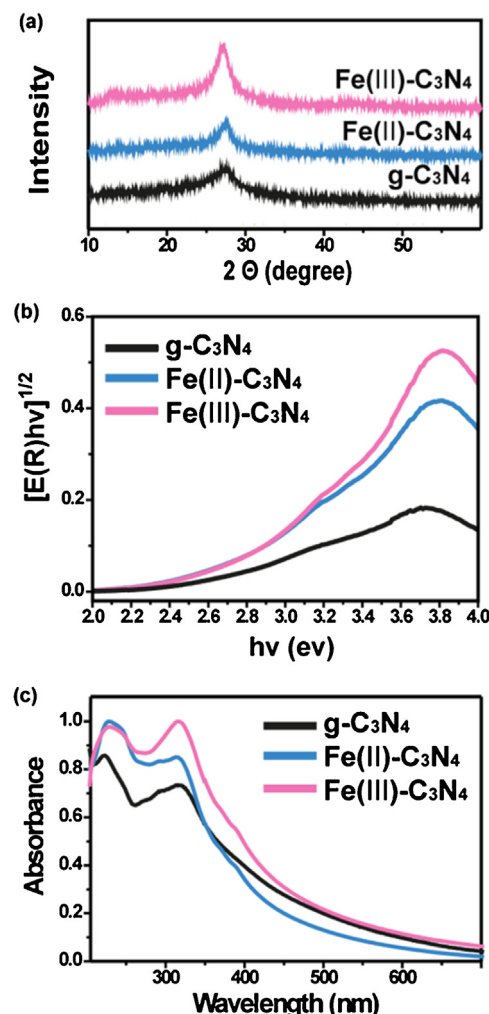


Fig. 1. (a) XRD data, (b) normalized UV-vis absorption spectra and (c) the $(E(R)hv)^{1/2}$ versus photon energy curves.

A value of n of $1/2$ was used in the present case, referring to allowed direct transitions [66]. Values of 2.5 eV, 2.4 eV, and 2.4 eV were determined for $\text{g-C}_3\text{N}_4$, $\text{Fe(II)-C}_3\text{N}_4$ and $\text{Fe(III)-C}_3\text{N}_4$, respectively.

$$\alpha h\nu = A(h\nu - E_g)^n/2 \quad (1)$$

The photocatalytic activity of $\text{g-C}_3\text{N}_4$, $\text{Fe(II)-C}_3\text{N}_4$ and $\text{Fe(III)-C}_3\text{N}_4$ in the degradation of PNP was assessed under UV and visible light illumination (Fig. 3). In each case the enhancement of the photocatalytic conversion with time corresponded to a gradual decrease of the concentration of PNP. Higher photocatalytic conversion levels were attained under UV light illumination. A lower recombination rate of photo-induced electron and hole pairs in the prepared Fe-doped catalysts was believed to result in an enhanced photocatalytic conversion. Similar reports focusing on an absorbance increase have claimed a subsequent enhancement in the generation of electron-hole pairs under light irradiation, resulting in a higher photocatalytic activity [67]. Despite the observed enhancement, the maximum conversion herein attained (ca. 40% after 5 h) was still considered to transpire a low photocatalytic activity of the evaluated samples. The limited efficiency of single component C_3N_4 samples therefore paves the interest of evaluating heterojunction-based $\text{C}_3\text{N}_4/\text{WO}_3$ hybrid structures in this study (Scheme 1).

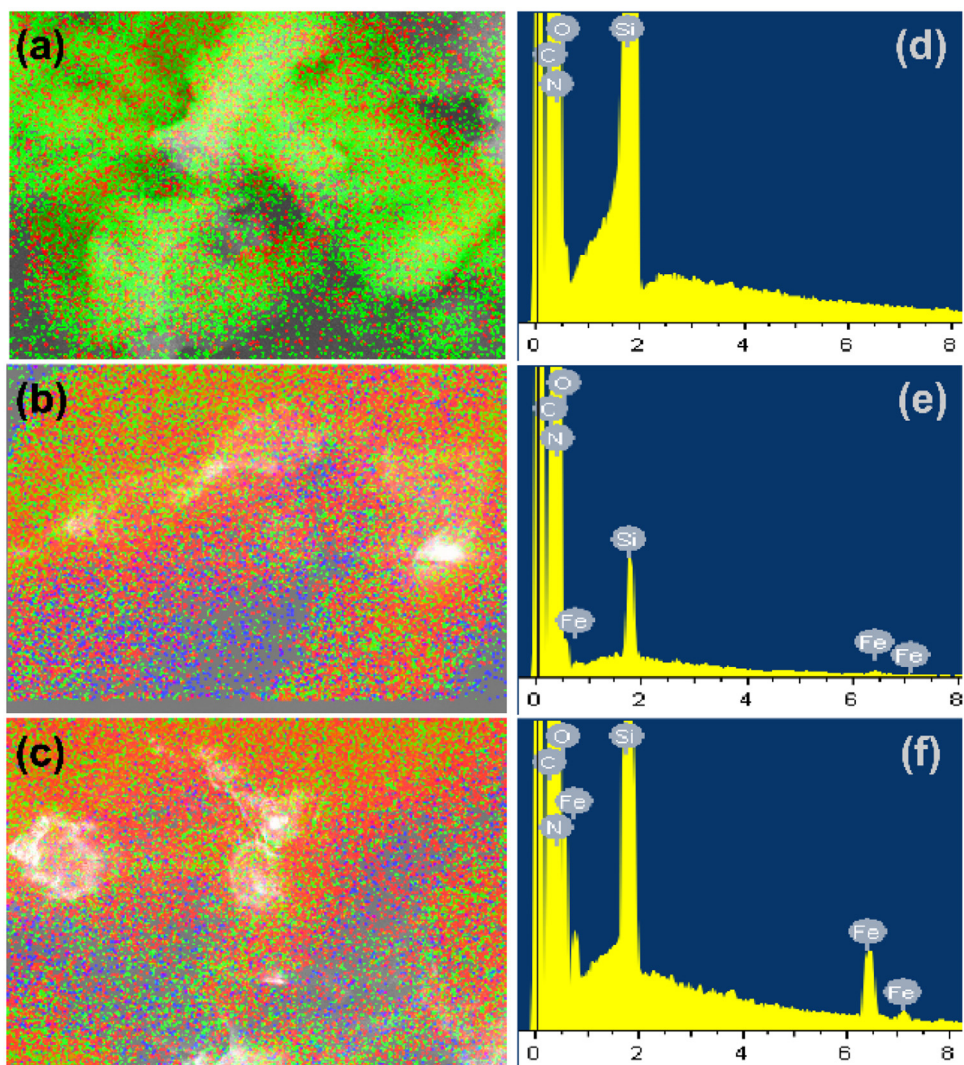


Fig. 2. Scanning electron microscopy and energy-dispersive X-ray spectroscopy (EDS) analysis. Elemental mapping of $\text{g-C}_3\text{N}_4$ (a, d), $\text{Fe}(\text{II})\text{-C}_3\text{N}_4$ (b, e) and $\text{Fe}(\text{III})\text{-C}_3\text{N}_4$ (c, f). (Red dot: N, Green dot: C, Blue dot: Fe). (For interpretation of the references to colour in this figure legend, the reader is referred to the web version of this article.)

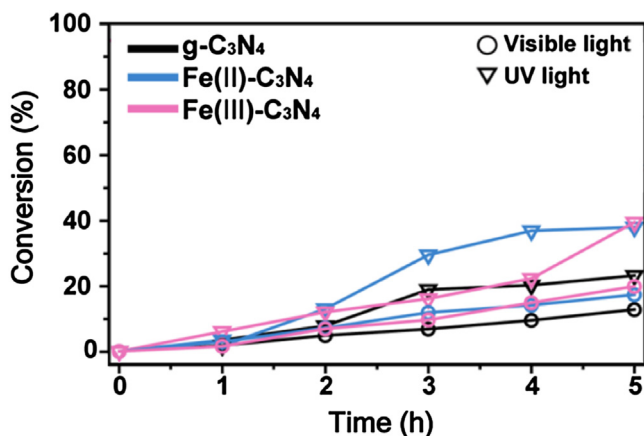


Fig. 3. Photocatalytic conversion for the degradation of PNP under visible and UV light illumination with $\text{g-C}_3\text{N}_4$ -based catalysts.

3.2. $\text{Fe-doped C}_3\text{N}_4/\text{WO}_3$ hybrid

XRD patterns of synthesized WO_3 nanostructure agreed with those referenced for the monoclinic WO_3 (JCPDF 43-1035) [68].

Similarly the hybrid structure revealed XRD peaks consistent with those of $\text{g-C}_3\text{N}_4$ and WO_3 (Fig. 4e). Representative TEM images of few nm-thick free-standing $\text{g-C}_3\text{N}_4$ nanosheets (Fig. 4a) agreed with corresponding AFM results discussed above (Fig. S3). WO_3 nanoparticles of 20–100 nm in diameter were attached to the surface of the C_3N_4 sheets (Fig. 4b–d). The lattice fringes of WO_3 evidenced in Fig. S6 were confirmed to correspond to the interplanar spacing of (220), (200), (020) and (002) lattice planes of monoclinic WO_3 (JCPDF 43-1035) [58]. Overall comparison of the morphology of all samples is displayed in Fig. S7. Additional HR-SEM photographs of the hybrid materials and individual elemental mapping underlined the successfulness of the synthesis with a uniform distribution of N, C, Fe and W (Fig. S8). The hybrid $\text{g-C}_3\text{N}_4/\text{WO}_3$ composites exhibited longer wavelengths absorption edges compared to $\text{g-C}_3\text{N}_4$ (Fig. 4f). The overall red shift of the absorption wavelength implies a higher absorption with the hybrid photocatalyst in the visible light range, and an enhanced formation of electron-hole pairs. Electrochemical impedance spectroscopy (EIS) was carried out to investigate the charge transfer resistance and the separation efficiency between the photogenerated species [69–73]. $\text{C}_3\text{N}_4/\text{WO}_3$ was confirmed to evidence lower resistance suggesting an enhanced separation and transfer efficiency of photogenerated electron-hole pairs, which is favorable for enhancing the activity

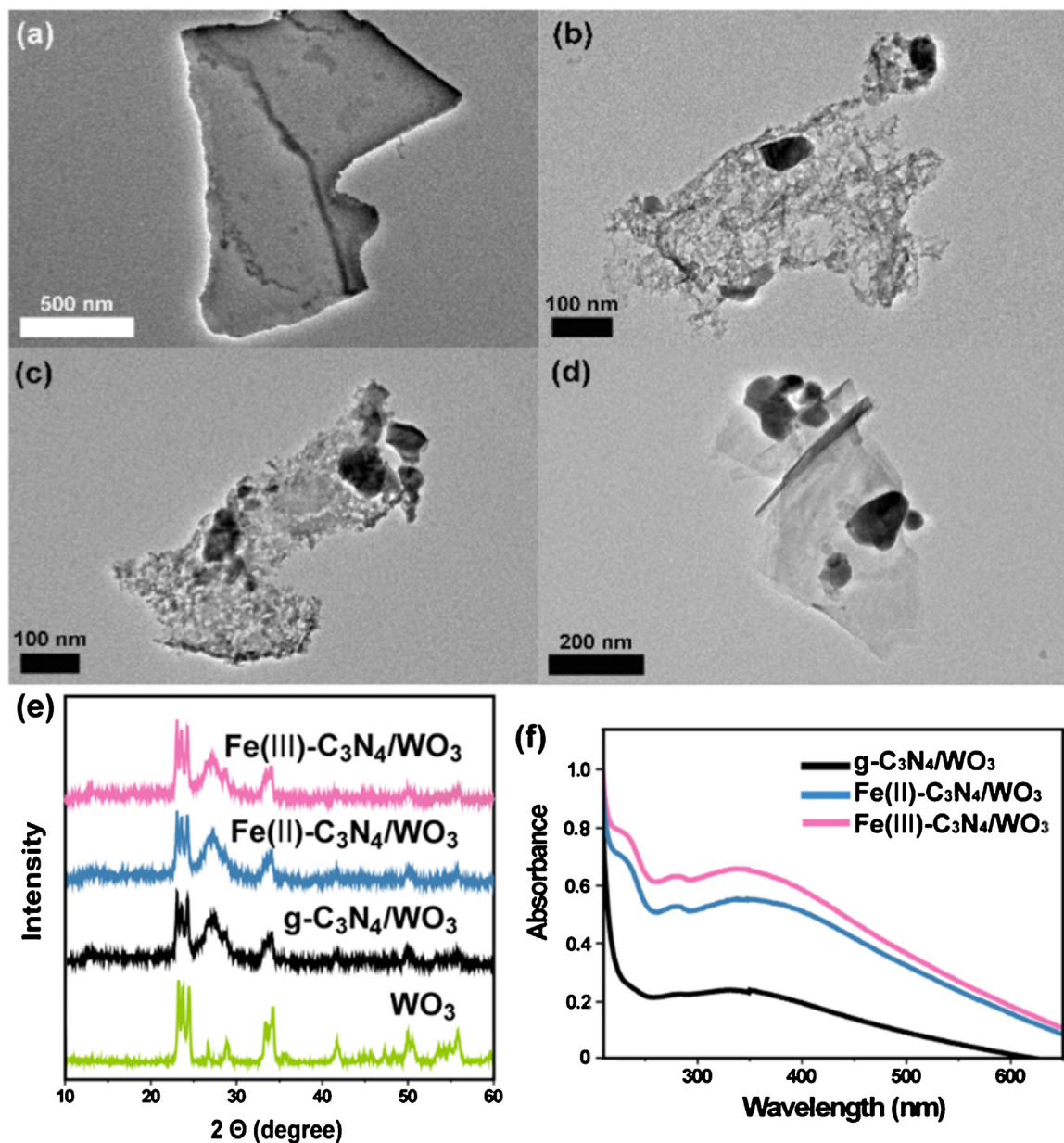


Fig. 4. TEM image of (a) g-C₃N₄ reference, (b) C₃N₄/WO₃, (c) Fe(II)-C₃N₄/WO₃ and (d) Fe(III)-C₃N₄/WO₃. (e) Collected XRD patterns for WO₃ and the prepared hybrid composites. (f) Normalized UV-vis absorption spectra.

in the reaction (Fig. S9). The result was in further agreement with previously published data [58].

The prepared g-C₃N₄/WO₃ hybrid photocatalytic systems were evaluated under visible light illumination and in presence of H₂O₂ as an oxidizing agent, for effective PNP degradation. Prior to the catalytic measurements, the effect of the amount of H₂O₂ on the degradation of PNP in the Photo-Fenton system was investigated (Fig. S10). A relatively low 0.005 M H₂O₂ concentration was found suitable in the present study. Resulting activities of the degradation of PNP based on simultaneous photo-oxidation and photo-Fenton reaction in presence of H₂O₂ have been summarized in Fig. 5. Conversion values of 43, 45 and 49% were obtained with C₃N₄/WO₃, Fe(II)-C₃N₄/WO₃ and Fe(III)-C₃N₄/WO₃, respectively. After 4 h of reaction a remarkable increase of activity from ca. 10% to ca. 40% was observed upon the introduction of WO₃ in the photocatalytic system. Aside from the expected photocatalytic contribution of WO₃, this impressive boost in activity is expected to be the result of

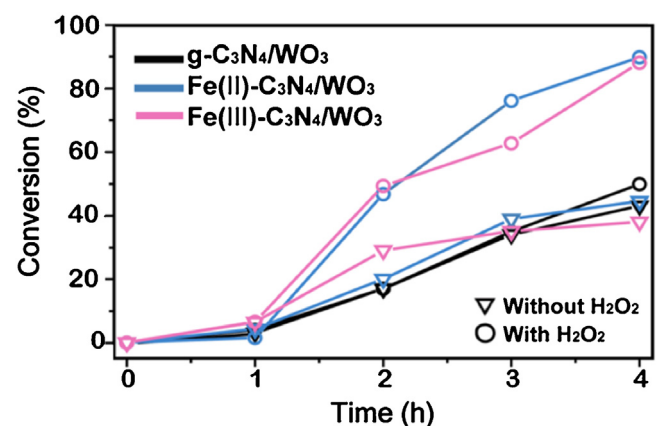


Fig. 5. Conversion (%) for the degradation of PNP under visible light illumination with all prepared samples, in the presence or absence of H₂O₂.

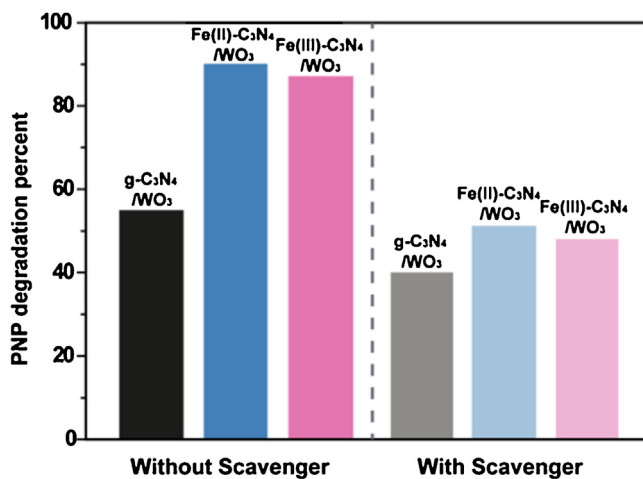


Fig. 6. Photo-Fenton reaction carried out in the presence and absence of a hydroxyl radicals scavenger agent (*tert*-butanol).

the improved separation of photo-induced electron and hole pairs by bandgap alignment hinted by the EIS results.

Whereas $\text{C}_3\text{N}_4/\text{WO}_3$ did not evidence an increase in the degradation of PNP upon the addition of H_2O_2 , the conversion was remarkably enhanced up to ca. 91 and 89% with both Fe(II)- and Fe(III)-doped $\text{C}_3\text{N}_4/\text{WO}_3$, respectively. It is underlined herein that the photocatalytic activity was maximized as a result of a synergism of the ‘Photo-Fenton cycle’ with Fe(II) or Fe(III) doping in the presence of H_2O_2 , which generated additional hydroxyl radicals. Further evidence of this Photo-Fenton reaction mechanism is provided in the following section. The samples were further compared upon irradiation under UV light (Fig. S11). In all cases, a significant enhancement of the activity was registered, in agreement with the results obtained with the Fe-doped C_3N_4 samples. The stability of the Fe-doped catalysts was assessed under visible light source to assure the applicability of the materials herein presented. Deactivation of both samples was considered negligible at the end of the performed tests as summarized in Table S1.

3.3. Further evidence of the photo-Fenton reaction mechanism

The significance of the presence of hydroxyl radicals in the photo-Fenton performance of Fe-doped $\text{C}_3\text{N}_4/\text{WO}_3$ was assessed through photocatalytic tests carried out in the presence of an OH radicals scavenger agent (Fig. 6). The degradation of PNP was determined after 4 h under visible light illumination, in the presence of *tert*-butyl alcohol (TBA). Both Fe-doped samples unveiled a striking decrease of the degradation percentage from ca. 90% to ca. 50%. Notably, the attained conversion in the presence of TBA was comparable to the value determined in the absence of H_2O_2 after 4 h, during the previously discussed tests (Fig. 5). Similar concluding remarks were drawn following collected photoluminescence data using terephthalic acid (TA). The relative concentration of hydroxyl radicals was compared according to the formation of 2-hydroxyterephthalic acid (TAOH) in the presence of OH radical species [64]. The formation of TAOH detected at 435 nm was remarkably enhanced after 3 h of reaction compared to the $\text{C}_3\text{N}_4/\text{WO}_3$ reference (Fig. 7).

Spin trapping enabled by electron paramagnetic resonance (EPR) analysis has been proved to be the most direct and sensitive approach to effectively detect the formed short-living OH radical species [54]. Whereas a minor focus has been attributed to its application in Photo-Fenton reactions, *in-situ* EPR with DMPO spin trap was herein found suitable to provide further evidence in the postulated reaction mechanism. Obtained results were summa-

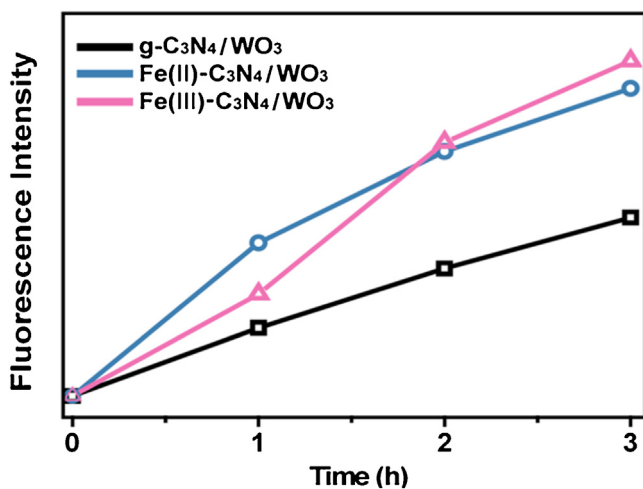


Fig. 7. Hydroxyl radicals trapping PL spectra in TA solution under visible light in presence of H_2O_2 .

rized in Fig. 8. The EPR spectrum exhibited a four-line pattern with intensity ratios of 1:2:2:1. Nitrogen and proton hyperfine coupling values corresponded to $A_N \sim 14.9$ G and $A_H \sim 14.9$ G, respectively. This clearly showed that the EPR signals arise from the DMPO-hydroxyl radical adduct [74]. The comparison of the magnitude of the EPR spectrum is representative of the amount of formed DMPO-hydroxyl radical species. In agreement with the aforementioned PNP degradation data, upon visible light illumination the DMPO-hydroxyl radical signal unveiled a remarkable enhancement up to 45 and 35% with Fe(II) and Fe(III)-doped catalysts, respectively. At the beginning of the Fenton process, the Fe(II) sample is believed to react faster than the Fe(III) counterpart, which could be attributed to two main reasons. First, the Fe(II) was consumed almost totally at the beginning and the conversion rate of the Fe(III) to the Fe(II) is relatively lower than the consumption rate of the Fe(II) [75]. The cyclic mechanism from $[\text{Fe}^{2+} + \text{H}_2\text{O}_2 \rightarrow \text{Fe}^{3+} + \text{OH}^- + \text{OH}^{\cdot}]$ additionally suggests that the Fe(II)-doped sample shows faster initial catalytic activity compared to the Fe(III) counterpart [76,77]. Following an initial Fe(II) consumption, the concentration of the latter could be further enhanced succeeding the reduction of Fe(III) under visible light illumination [45,78]. The EPR result of the Fe(III) doped sample in Fig. 8 proves the mechanism which was induced by photo-generated electron. In good agreement, both Fe-doped catalysts exhibited similar conversion efficiency levels after 4 h in the degradation of PNP under visible light illumination (Fig. 5).

The studies *via in-situ* EPR, scavenger test and photoluminescence were able to shed additional light in the postulated mechanism for PNP degradation in the presence of Fe-doped $\text{C}_3\text{N}_4/\text{WO}_3$ hybrid catalysts. The mechanism representing electron and hole separation and corresponding transfer in the hybrid $\text{C}_3\text{N}_4/\text{WO}_3$ structure under visible light illumination has been illustrated in Scheme 2. In accordance, upon the absorption of photons, when the WO_3 nanoparticles are combined with $\text{g-C}_3\text{N}_4$, the photo-induced electrons in the conduction band (CB) of $\text{g-C}_3\text{N}_4$ (-1.13 eV) can be readily transferred into WO_3 (0.75 eV). Similarly, the photo-induced holes in the valence band (VB) of WO_3 (3.44 eV) are easily transferred to $\text{g-C}_3\text{N}_4$ (1.57 eV) [57]. By effectively suppressing the electron-hole recombination [79,80], PNP degradation could be notably enhanced. The excited-electrons directly injected into the CB of WO_3 are expected to be further transferred to Fe(III) (Eqs. (2) and (3)). Simultaneously, the holes in the VB of WO_3 transferred to $\text{g-C}_3\text{N}_4$ are assumed to react with H_2O_2 to produce hydroxyl radicals (Eq. (4)). The proposed mechanism is therefore expected

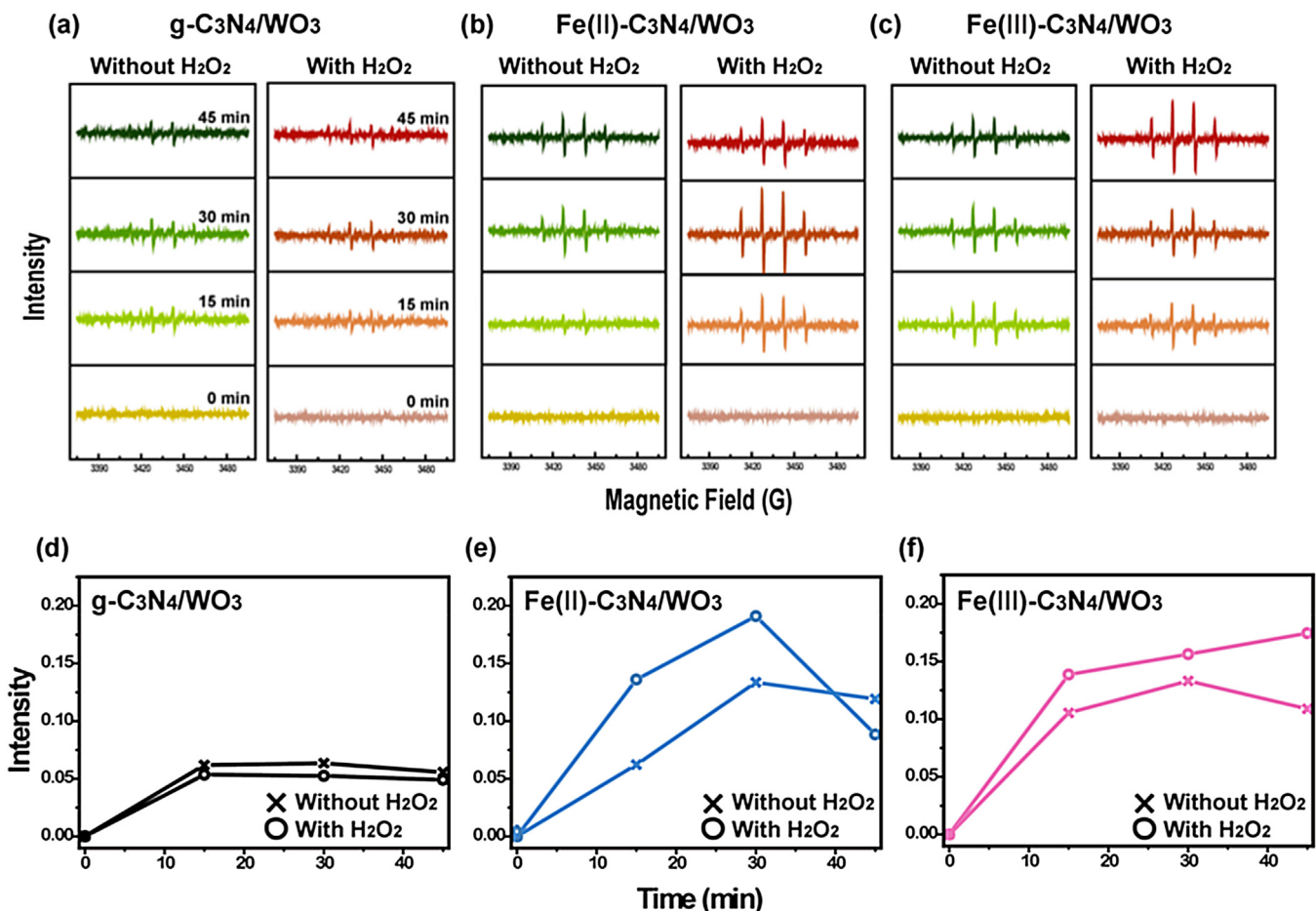
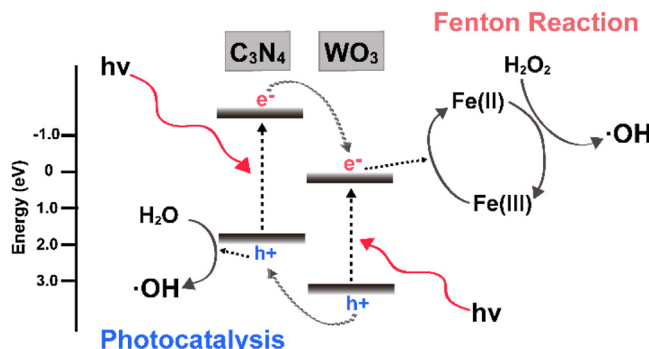


Fig. 8. Real time measured Electron paramagnetic resonance (EPR) spectra of hydroxyl radicals trapped by DMPO. Results obtained with (a) C₃N₄/WO₃, (b) Fe(II)-C₃N₄/WO₃ and (c) Fe(III)-C₃N₄/WO₃ under visible light illumination.



Scheme 2. Schematic illustration of the Photo-Fenton process representing electron and hole separation and transfer in the hybrid structure under visible light irradiation.

to produce more hydroxyl radicals in comparison with both photocatalysis and the Fenton reaction operating individually. This enhancement, accelerated by electrons and holes, is hence in good agreement with the results herein obtained.



4. Conclusions

In this contribution we suggest a viable and efficient photocatalytic system with prominent performance utilizing a photo-Fenton reaction for innovative solar energy conversion based on Fe-doped C₃N₄/WO₃ composites. In the degradation of PNP, our novel Fe-doped C₃N₄/WO₃ hybrid catalysts unveiled a striking enhancement of the conversion efficiency up to ca. 90% after 4 h compared with the evaluated g-C₃N₄ reference (ca. 10%) after the same period of time. EIS confirmed an increased separation efficiency between photogenerated species in presence of the C₃N₄/WO₃ heterojunction. *In-situ* EPR analysis, scavenger test and fluorescence measurement were employed to shed additional light in the proposed detailed mechanism conveniently schematized in **Scheme 2**. It was concluded that the photo-induced electrons could promote the Fenton reaction, whereas the generated hydroxyl radicals could remarkably improve the catalytic activity. The comprehensive analysis of the obtained data is believed to extend our understanding in the Fe-mediated Fenton cycle as an efficient strategy to improve the catalytic performance. Accordingly, this contribution is expected to underline the potential of these materials in further practical applications in energy and environmental issues.

Acknowledgments

This work was supported by National Research Foundation of Korea Grant funded by the Korean Government

(2014R1A2A1A09005656; 2013K2A5A6060972; 2011-0030255), and by the National Research Council of Science and Technology through the Degree & Research Center Program (DRC-2014-1-KBSI; DRC-2014-3-KBSI). Y. Oh and S. O. Kim acknowledge the financial support by Nano-Material Technology Development Program through the National Research Foundation of Korea (NRF) funded by the Ministry of Science, ICT and Future Planning (NRF-2016M3A7B4905613).

Appendix A. Supplementary data

Supplementary data associated with this article can be found, in the online version, at <http://dx.doi.org/10.1016/j.apcatb.2017.01.038>.

References

- [1] W. Hou, S.B. Cronin, *Adv. Funct. Mater.* 23 (2013) 1612–1619.
- [2] Y. Wang, Q. Wang, X. Zhan, F. Wang, M. Safdar, J. He, *Nanoscale* 5 (2013) 8326–8339.
- [3] S.T. Kochuveedu, Y.J. Jang, Y.H. Jang, W.J. Lee, M.-A. Cha, H. Shin, S. Yoon, S.-S. Lee, S.O. Kim, K. Shin, M. Steinhart, D.H. Kim, *Green Chem.* 13 (2011) 3397–3405.
- [4] Q. Xiang, J. Yu, M. Jaroniec, *Chem. Soc. Rev.* 41 (2012) 782–796.
- [5] M. Yoon, J.-E. Lee, Y.J. Jang, J.W. Lim, A. Rani, D.H. Kim, *ACS Appl. Mater. Interfaces* 7 (2015) 21073–21081.
- [6] L.N. Quan, Y.H. Jang, K.A. Stoerzinger, K.J. May, Y.J. Jang, S.T. Kochuveedu, Y. Shao-Horn, D.H. Kim, *Phys. Chem. Chem. Phys.* 16 (2014) 9023–9030.
- [7] S.T. Kochuveedu, Y.H. Jang, D.H. Kim, *Chem. Soc. Rev.* 42 (2013) 8467–8493.
- [8] H.G. Yang, C.H. Sun, S.Z. Qiao, J. Zou, G. Liu, S.C. Smith, H.M. Cheng, G.Q. Lu, *Nature* 453 (2008) 638–641.
- [9] Y.W. Cheng, R.C.Y. Chan, P.K. Wong, *Water Res.* 41 (2007) 842–852.
- [10] J.H. Park, S. Kim, A.J. Bard, *Nano Lett.* 6 (2006) 24–28.
- [11] M. Msibi, S. Rossignol, J.-M. Tatibouët, C. Trapalis, *Mater. Lett.* 62 (2008) 4204–4206.
- [12] S.T. Kochuveedu, Y.H. Jang, Y.J. Jang, D.H. Kim, *J. Mater. Chem. A* 1 (2013) 898–905.
- [13] J. Yu, J. Xiong, B. Cheng, S. Liu, *Appl. Catal. B: Environ.* 60 (2005) 211–221.
- [14] K. Woan, G. Pyrgiotakis, W. Sigmund, *Adv. Mater.* 21 (2009) 2233–2239.
- [15] M.-A. Cha, C. Shin, D. Kannaiyan, Y.H. Jang, S.T. Kochuveedu, D.Y. Ryu, D.H. Kim, *J. Mater. Chem.* 19 (2009) 7245–7250.
- [16] D. Kannaiyan, E. Kim, N. Won, K.W. Kim, Y.H. Jang, M.-A. Cha, D.Y. Ryu, S. Kim, D.H. Kim, *J. Mater. Chem.* 20 (2010) 677–682.
- [17] W.J. Lee, J.M. Lee, S.T. Kochuveedu, T.H. Han, H.Y. Jeong, M. Park, J.M. Yun, J. Kwon, K. No, D.H. Kim, S.O. Kim, *ACS Nano* 6 (2012) 935–943.
- [18] J. Yu, J. Zhang, M. Jaroniec, *Green Chem.* 12 (2010) 1611–1614.
- [19] Y. Zhu, Y. Wang, Q. Ling, Y. Zhu, *Appl. Catal. B: Environ.* 200 (2017) 222–229.
- [20] H. Yang, J. Tian, T. Li, H. Cui, *Catal. Commun.* 87 (2016) 82–85.
- [21] M. Zhang, W. Luo, Z. Wei, W. Jiang, D. Liu, Y. Zhu, *Appl. Catal. B: Environ.* 194 (2016) 105–110.
- [22] N. Wei, H. Cui, Q. Song, L. Zhang, X. Song, K. Wang, Y. Zhang, J. Li, J. Wen, J. Tian, *Appl. Catal. B: Environ.* 198 (2016) 83–90.
- [23] J. Oh, S. Lee, K. Zhang, J.O. Hwang, J. Han, G. Park, S.O. Kim, J.H. Park, S. Park, *Carbon* 66 (2014) 119–125.
- [24] H. Zhao, H. Yu, X. Quan, S. Chen, Y. Zhang, H. Zhao, H. Wang, *Appl. Catal. B: Environ.* 152–153 (2014) 46–50.
- [25] H. Liu, D. Chen, Z. Wang, H. Jing, R. Zhang, *Appl. Catal. B: Environ.* 203 (2017) 300–313.
- [26] L. Liu, Y. Qi, J. Lu, S. Lin, W. An, Y. Liang, W. Cui, *Appl. Catal. B: Environ.* 183 (2016) 133–141.
- [27] C. Lu, P. Zhang, S. Jiang, X. Wu, S. Song, M. Zhu, Z. Lou, Z. Li, F. Liu, Y. Liu, Y. Wang, Z. Le, *Appl. Catal. B: Environ.* 200 (2017) 378–385.
- [28] L. Liu, Y. Qi, J. Hu, Y. Liang, W. Cui, *Appl. Surf. Sci.* 351 (2015) 1146–1154.
- [29] L. Liu, Y. Qi, J. Hu, W. An, S. Lin, Y. Liang, W. Cui, *Mater. Lett.* 158 (2015) 278–281.
- [30] L. Liu, Y. Qi, J. Yang, W. Cui, X. Li, Z. Zhang, *Appl. Surf. Sci.* 358 (2015) 319–327.
- [31] L. Liu, Y. Qi, J. Lu, S. Lin, W. An, J. Hu, Y. Liang, W. Cui, *RSC Adv.* 5 (2015) 99339–99346.
- [32] A. Vinu, *Adv. Funct. Mater.* 18 (2008) 816–827.
- [33] S.N. Talapaneni, S. Anandan, G.P. Mane, C. Anand, D.S. Dhawale, S. Varghese, A. Mano, T. Mori, A. Vinu, *J. Mater. Chem.* 22 (2012) 9831–9840.
- [34] G. Zhang, M. Zhang, X. Ye, X. Qiu, S. Lin, X. Wang, *Adv. Mater.* 26 (2014) 805–809.
- [35] Q. Li, J. Yang, D. Feng, Z. Wu, Q. Wu, S. Park, C.-S. Ha, D. Zhao, *Nano Res.* 3 (2010) 632–642.
- [36] S. Yang, Y. Gong, J. Zhang, L. Zhan, L. Ma, Z. Fang, R. Vajtai, X. Wang, P.M. Ajayan, *Adv. Mater.* 25 (2013) 2452–2456.
- [37] Z. Ding, X. Chen, M. Antonietti, X. Wang, *ChemSusChem* 4 (2011) 274–281.
- [38] D.H. Lee, W.J. Lee, W.J. Lee, S.O. Kim, Y.-H. Kim, *Phys. Rev. Lett.* 106 (2011) 175502.
- [39] S. Kumar, T. Surendar, A. Baruah, V. Shanker, *J. Mater. Chem. A* 1 (2013) 5333–5340.
- [40] Y. Zhang, T. Mori, L. Niu, J. Ye, *Energ. Environ. Sci.* 4 (2011) 4517–4521.
- [41] Y. Wang, H. Li, J. Yao, X. Wang, M. Antonietti, *Chem. Sci.* 2 (2011) 446–450.
- [42] J. Sun, J. Zhang, M. Zhang, M. Antonietti, X. Fu, X. Wang, *Nat. Commun.* 2 (2012) 1139.
- [43] Y. Wang, R. Shi, J. Lin, Y. Zhu, *Energ. Environ. Sci.* 4 (2011) 2922–2929.
- [44] F. Su, S.C. Mathew, L. Möhlmann, M. Antonietti, X. Wang, S. Blechert, *Angew. Chem. Int. Ed.* 50 (2011) 657–660.
- [45] C. Vilchèze, T. Hartman, B. Weinrick, W.R. Jacobs, *Nat. Commun.* 4 (2013) 1881.
- [46] R. Gonzalez-Olmos, M.J. Martin, A. Georgi, F.-D. Kopinke, I. Oller, S. Malato, *Appl. Catal. B: Environ.* 125 (2012) 51–58.
- [47] R. Gonzalez-Olmos, F. Holzer, F.D. Kopinke, A. Georgi, *Appl. Catal. A: Gen.* 398 (2011) 44–53.
- [48] H. Bataineh, O. Pestovsky, A. Bakac, *Chem. Sci.* 3 (2012) 1594–1599.
- [49] Y. Baba, T. Yatagai, T. Harada, Y. Kawase, *Chem. Eng. J. (Lausanne)* 277 (2015) 229–241.
- [50] C. Chen, Y. Zhou, N. Wang, L. Cheng, H. Ding, *RSC Adv.* 5 (2015) 95523–95531.
- [51] X. Yang, W. Chen, J. Huang, Y. Zhou, Y. Zhu, C. Li, *Sci. Rep.* 5 (2015) 10632.
- [52] W. Kim, T. Tachikawa, G.-h. Moon, T. Majima, W. Choi, *Angew. Chem. Int. Ed.* 53 (2014) 14036–14041.
- [53] C. Liu, R. Roder, L. Zhang, Z. Ren, H. Chen, Z. Zhang, C. Ronning, P.-X. Gao, *J. Mater. Chem. A* 2 (2014) 4157–4167.
- [54] Y. Luo, X.-r. Wang, L.-l. Ji, Y. Su, *J. Hazard. Mater.* 171 (2009) 1096–1102.
- [55] Y. Oh, J.O. Hwang, E.-S. Lee, M. Yoon, V.-D. Lee, Y.-H. Kim, D.H. Kim, S.O. Kim, *ACS Appl. Mater. Interfaces* 8 (38) (2016) 25438–25443, <http://dx.doi.org/10.1021/acsami.6b07287>.
- [56] P. Zhang, X. Hou, L. Liu, J. Mi, M. Dong, *J. Phys. Chem. C* 119 (2015) 28028–28037.
- [57] D. Jiang, L. Chen, J. Zhu, M. Chen, W. Shi, J. Xie, *Dalton Trans.* 42 (2013) 15726–15734.
- [58] L. Huang, H. Xu, Y. Li, H. Li, X. Cheng, J. Xia, Y. Xu, G. Cai, *Dalton Trans.* 42 (2013) 8606–8616.
- [59] H. Ji, X. Jing, Y. Xu, J. Yan, H. Li, Y. Li, L. Huang, Q. Zhang, H. Xu, H. Li, *RSC Adv.* 5 (2015) 57960–57967.
- [60] L. Yang, S. Luo, Y. Li, Y. Xiao, Q. Kang, Q. Cai, *Environ. Sci. Technol.* 44 (2010) 7641–7646.
- [61] Y. Yu, T. He, L. Guo, Y. Yang, L. Guo, Y. Tang, Y. Cao, *Sci. Rep.* 5 (2015) 9561.
- [62] J. Kim, C.W. Lee, W. Choi, *Environ. Sci. Technol.* 44 (2010) 6849–6854.
- [63] Y. Zhang, N. Zhang, Z.-R. Tang, Y.-J. Xu, *Chem. Sci.* 4 (2013) 1820–1824.
- [64] K.-i. Ishibashi, A. Fujishima, T. Watanabe, K. Hashimoto, *Electrochim. Commun.* 2 (2000) 207–210.
- [65] X. Wang, K. Maeda, A. Thomas, K. Takanabe, G. Xin, J.M. Carlsson, K. Domen, M. Antonietti, *Nat. Mater.* 8 (2009) 76–80.
- [66] T.I. Nkambule, A.T. Kuvaruga, R.W.M. Krause, J. Haarhoff, B.B. Mamba, *Environ. Sci. Pollut. Res.* 19 (2012) 4120–4132.
- [67] S. Tonda, S. Kumar, S. Kandula, V. Shanker, *J. Mater. Chem. A* 2 (2014) 6772–6780.
- [68] I.M. Szilágyi, B. Fórizs, O. Rosseler, Á. Szegedi, P. Németh, P. Király, G. Tárkányi, B. Vajna, K. Varga-Josepovits, K. László, A.L. Tóth, P. Baranyai, M. Leskelä, *J. Catal.* 294 (2012) 119–127.
- [69] P. Tan, X. Chen, L. Wu, Y.Y. Shang, W. Liu, J. Pan, X. Xiong, *Appl. Catal. B: Environ.* 202 (2017) 326–334.
- [70] L. Liu, L. Ding, Y. Liu, W. An, S. Lin, Y. Liang, W. Cui, *Appl. Catal. B: Environ.* 201 (2017) 92–104.
- [71] Y. Liang, S. Lin, L. Liu, J. Hu, W. Cui, *Appl. Catal. B: Environ.* 164 (2015) 192–203.
- [72] W. Cui, W. An, L. Liu, J. Hu, Y. Liang, J. Hazard. Mater. 280 (2014) 417–427.
- [73] W. Cao, Z. Gui, L. Chen, X. Zhu, Z. Qi, *Appl. Catal. B: Environ.* 200 (2017) 681–689.
- [74] M.A. Voinov, J.O.S. Pagán, E. Morrison, T.I. Smirnova, A.I. Smirnov, *J. Am. Chem. Soc.* 133 (2011) 35–41.
- [75] L. Guo, F. Chen, X. Fan, W. Cai, J. Zhang, *Appl. Catal. B: Environ.* 96 (2010) 162–168.
- [76] V. Kavitha, K. Palanivelu, *Chemosphere* 55 (2004) 1235–1243.
- [77] G. Ruppert, R. Bauer, G. Heisler, *Chemosphere* 28 (1994) 1447–1454.
- [78] S.M. Kim, A. Vogelpohl, *Chem. Eng. Technol.* 21 (1998) 187–191.
- [79] J. Fang, H. Fan, M. Li, C. Long, *J. Mater. Chem. A* 3 (2015) 13819–13826.
- [80] Y. Hou, F. Zuo, A.P. Dagg, J. Liu, P. Feng, *Adv. Mater.* 26 (2014) 5043–5049.